Exact low-temperature properties of a class of highly frustrated Hubbard models

Oleg Derzhko,[1,2] Andreas Honecker,[3] and Johannes Richter[2]
[1]*Institute for Condensed Matter Physics, National Academy of Sciences of Ukraine, L'viv-11, 79011, Ukraine*
[2]*Institut für Theoretische Physik, Universität Magdeburg, P.O. Box 4120, 39016 Magdeburg, Germany*
[3]*Institut für Theoretische Physik, Georg-August-Universität Göttingen, 37077 Göttingen, Germany*
(Received 7 November 2008; published 2 February 2009)

We study the repulsive Hubbard model both analytically and numerically on a family of highly frustrated lattices which have one-electron states localized on isolated trapping cells. We construct and count exact many-electron ground states for a wide range of electron densities and obtain closed-form expressions for the low-temperature thermodynamic quantities which are universal for all lattices of the family. Furthermore, we find that saturated ferromagnetism is obtained only for sufficiently high electron densities and large Hubbard repulsion U while there is no finite average moment in the ground states at lower densities.

DOI: 10.1103/PhysRevB.79.054403 PACS number(s): 75.10.Lp, 71.10.Fd

I. INTRODUCTION

Exactly solvable interacting quantum lattice systems are of great importance in condensed-matter physics. Although most of the examples are known for one-dimensional systems, two-dimensional and three-dimensional models are also coming into sight. A crucial point in searching for exactly solvable lattice models concerns the lattice geometry. Furthermore the interplay between lattice geometry, interactions, and quantum fluctuations often gives rise to exotic quantum phases. Famous examples where a special arrangement of interaction bonds allows to find exact quantum many-body ground states are the Majumdar-Ghosh model,[1] the Shastry-Sutherland model,[2] and the Kitaev model.[3]

Besides revealing new magnetic properties of previously known materials (e.g., the diamond-chain compound azurite[4]) there are presently various possibilities to design interacting lattice systems with controlled geometry. Modern strategies in chemistry open a route to synthesize new materials with a desired lattice structure and intersite interactions.[5,6] Moreover, recent progress in nanotechnology allows the fabrication of quantum dot superlattices and quantum wire systems with any type of lattice.[7] Another rapidly developing field is the controlled setup of optical lattices for cold atoms.[8,9]

Motivated by these achievements we propose here a class of lattices (including the well-known diamond chain, frustrated ladder, square-kagome, and checkerboard lattices) for which various properties of the Hubbard model can be examined rigorously. In particular, we characterize the complete manifold of highly degenerate ground states for electron numbers $n=1,\ldots,\mathcal{N}\propto N$ and calculate low-temperature thermodynamic quantities around a particular value of the chemical potential μ_0. The general lattice construction rules illustrated below are based on a local point of view similar (but not identical) to earlier considerations for electronic[10,11] and spin systems.[12] Below we also discuss some properties of the Hubbard model for a few one-dimensional and two-dimensional representatives. We illustrate the dominating role of the exact ground states for the low-temperature physics of the Hubbard model at certain electron densities. Furthermore we analyze the ground state with respect to magnetic properties. We confirm our analytical findings by numerical data for finite systems.

II. LATTICES WITH TRAPPING CELLS

We consider the N-site Hubbard Hamiltonian

$$H=\sum_{\sigma=\uparrow,\downarrow} H_{0\sigma}+H_U, \quad H_U=U\sum_i n_{i,\uparrow}n_{i,\downarrow},$$

$$H_{0\sigma}=\sum_{\langle i,j\rangle} t_{i,j}(c^{\dagger}_{i,\sigma}c_{j,\sigma}+c^{\dagger}_{j,\sigma}c_{i,\sigma})+\mu\sum_i n_{i,\sigma}, \tag{1}$$

where i denotes the lattice sites, $\langle i,j\rangle$ denote the bonds connecting neighboring sites, the $c^{\dagger}_{i,\sigma}$ $(c_{i,\sigma})$ are the usual fermion operators, $n_{i,\sigma}=c^{\dagger}_{i,\sigma}c_{i,\sigma}$, $t_{i,j}>0$ are the hopping integrals, $U\geq 0$ is the on-site Coulomb repulsion, and μ is the chemical potential.

We consider the Hubbard model (1) on a family of lattices defined by the following construction rules: (i) Take a "trapping cell", i.e., a finite region where an electron in the infinite lattice will be localized. For simplicity, we consider here bipartite cells with equivalent sites and bonds, such as a single bond between two sites, equilateral even polygons, or a cube.[13] (ii) Solve the one-electron problem for the trapping cell, finding the lowest-energy eigenfunction $\propto\Sigma_i a_i c^{\dagger}_{i,\sigma}|0\rangle$ with $|0\rangle$ denoting the vacuum state. For traps consisting of a single bond or a square the ground state is nondegenerate and $a_1=-a_2=1$ or $a_1=-a_2=a_3=-a_4=1$, respectively. (iii) Arrange the trapping cells into a regular pattern so that trapping cells do not touch each other (do not have common sites) and complete the lattice by connecting the cells via surrounding (connecting) bonds. Most importantly, the connecting bond scheme should prevent the escape of the localized electron from the trap, i.e., the constructed one-electron (localized) state should remain an eigenstate of the Hamiltonian on the infinite lattice. It is easy to show that a sufficient condition for this is $\Sigma_i t_{r,i}a_i=0$, where the sum runs over all sites i of a trapping cell and r is an arbitrary site which does not belong to the trap, see also Ref. 12. For such traps as a single bond, square, or cube this condition is fulfilled if an arbitrary bond of the trapping cell and the surrounding bonds attached to the

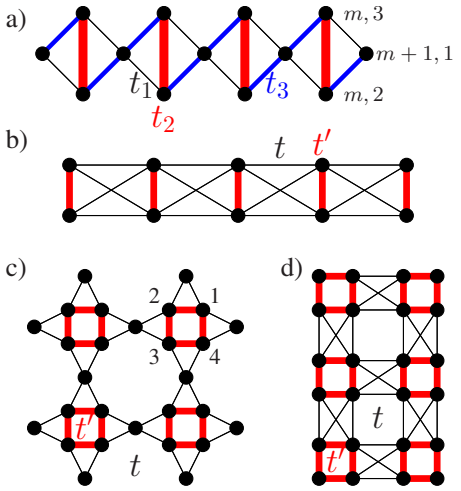

FIG. 1. (Color online) (a) Diamond chain, (b) frustrated ladder, (c) square-kagome, and (d) checkerboard lattices. The circles indicate the lattice sites, the thick (thin) lines indicate the hopping paths along the trap (connecting) bonds. For the ideal diamond chain with $t_1=t_3$ we will use the notation $t=t_1=t_3$, $t'=t_2$.

two sites of this bond form an isosceles triangle. (iv) Choose the hopping integrals t' of the trapping cells sufficiently large, $t'>t'_c$, so that the localized states become the lowest-energy ones in comparison with other (extended) one-electron states.

Following the rules formulated above we are able to construct many different one-dimensional, two-dimensional, and even three-dimensional lattices. Note that a lattice constructed in this manner has a flat one-electron band which for $t'>t'_c$ becomes the lowest-energy one. However, we emphasize that such lattices do not belong to Tasaki's models for flat-band ferromagnetism.[10]

In what follows we focus for concreteness on some typical representatives which were investigated in the context of strongly correlated systems earlier, namely, the diamond chain,[14] the frustrated ladder,[15,16] the square-kagome, and checkerboard lattices[12,17] (see Fig. 1). It is also convenient to denote sites by m, p, where $m=1,\ldots,\mathcal{N}$ denotes unit cells ($\mathcal{N}=N/3$, $N/2$, $N/6$, $N/4$ for the diamond chain, frustrated ladder, square-kagome, and checkerboard lattices, respectively) and p denotes sites inside the unit cell (see Fig. 1). Note that for the lattices considered here the number of unit cells is identical to the number of trapping cells. However, the trapping cell may or may not be identical to the unit cell.

III. LOCALIZED-ELECTRON STATES FOR $U=0$ AND $U>0$

Next we turn to the characterization of the complete manifold of highly degenerate ground states for electron numbers $n=1,\ldots,\mathcal{N}\propto N$. We start with the case $U=0$ considering the diamond chain with $t=t_1=t_3$, $t'=t_2$ for concreteness. Three one-electron bands,

$$\varepsilon_1-\mu=-t',$$

$$\varepsilon_{2,3}(\kappa)-\mu=\frac{t'}{2}\mp\sqrt{\left(\frac{t'}{2}\right)^2+4t^2(1+\cos\kappa)}, \qquad (2)$$

are arranged as follows for $t'>t'_c=2t$: $\varepsilon_1<\varepsilon_2(\kappa)<\varepsilon_3(\kappa)$. Note that the lowest one-electron band ε_1 is completely flat, i.e., κ independent. The corresponding states can be localized in real space. We introduce the operators $l^\dagger_{m,\sigma}=c^\dagger_{m,2,\sigma}-c^\dagger_{m,3,\sigma}$ [indices 2 and 3 denote the bottom and top sites on the vertical bond (see Fig. 1), m enumerates the unit cells] which satisfy $[H_{0\sigma},l^\dagger_{m,\sigma}]_-=\varepsilon_1 l^\dagger_{m,\sigma}$. Then all $2\mathcal{N}$ one-electron states belonging to the flat band can be written as $l^\dagger_{m,\sigma}|0\rangle$. Application of n distinct operators $l^\dagger_{m,\sigma}$ to $|0\rangle$ yields n-electron states with energy $E_n=n\varepsilon_1$, $n=1,\ldots,\mathcal{N}$. Note that all trapping cells are disconnected and the degeneracy of these n-electron states is

$$g^{(0)}_{\mathcal{N}}(n)=\binom{2\mathcal{N}}{n}. \qquad (3)$$

These arguments can be applied to other models: for the energy of the flat band $\varepsilon_1-\mu$ we find $-t'$, $-2t'$, $-2t'$ for the frustrated ladder, square-kagome, and checkerboard lattices, respectively. We assume $t'/t>t'_c/t=2,1,1$ for the frustrated ladder, square-kagome, and checkerboard lattices, respectively. For the square-kagome and checkerboard lattices an electron may be localized on smallest-area squares and $l^\dagger_{m,\sigma}=c^\dagger_{m,1,\sigma}-c^\dagger_{m,2,\sigma}+c^\dagger_{m,3,\sigma}-c^\dagger_{m,4,\sigma}$, where the indices 1,…,4 denote the vertices of the square.

We now address the case $U>0$. Since H_U is a positive semidefinite operator for $U>0$, it can only increase energies. The states for which each trapping cell contains up to one electron are exact eigenstates of the full Hamiltonian (1) with the U-independent energy $E_n=n\varepsilon_1$ and thus they remain the ground states in the subspaces $n=2,\ldots,\mathcal{N}$ in the presence of a Hubbard repulsion $U>0$. It is straightforward to count these localized n-electron ground states and we find

$$g_{\mathcal{N}}(n)=2^n\binom{\mathcal{N}}{n}<g^{(0)}_{\mathcal{N}}(n). \qquad (4)$$

The localized n-electron states are linearly independent which can be proven using the arguments of Ref. 18 (orthogonal class in the nomenclature of that reference). These states are the only ground states in each subspace $n=1,\ldots,\mathcal{N}$. This can be seen by recalling from spin systems that a finite separation of the flat one-particle band from the next (dispersive) band ensures completeness of the localized states.[17] For the present models, we can even control the energy gap by varying t'/t, in contrast to the sawtooth Hubbard chain.[19] The state with $\mathcal{N}$ electrons possesses perfect charge ordering (each trapping cell is occupied by precisely one electron) and therefore it can be understood as a particular realization of a Wigner crystal.[9] However, with respect to the spin orientations it has a huge degeneracy $2^{\mathcal{N}}$ (compare the degeneracy of the ground state, $\mathcal{N}+1$, at quarter filling when $n=\mathcal{N}$ for the sawtooth chain[10,19]).

IV. THERMODYNAMICS

The localized-electron ground states in the sectors with $n\leq\mathcal{N}$ have important implications for the low-temperature

properties of the Hubbard model (1) around a chemical potential $\mu_0=\mu-\varepsilon_1$; due to their huge degeneracy they dominate the grand-canonical partition function at low temperatures. Knowing the degeneracy [Eq. (4)] of the ground states $g_{\mathcal{N}}(n)$ and their energy $E_n=n\varepsilon_1$ we can write the grand-canonical partition function as

$$\Xi(T,\mu,N)=\sum_{n=0}^{\mathcal{N}} g_{\mathcal{N}}(n)e^{-n\varepsilon_1/T}=(1+2e^{-\varepsilon_1/T})^{\mathcal{N}}. \quad (5)$$

Note that only the combination $x=-\varepsilon_1/T=(\mu_0-\mu)/T$ enters the localized-electron contribution to any thermodynamic quantity. The thermodynamic potential becomes $\Omega(T,\mu,N)/\mathcal{N}=-T\ln(1+2\exp x)$ (the rhs is valid for both finite N and $N\to\infty$) leading to simple expressions for thermodynamic quantities such as

$$\frac{\bar{n}(T,\mu,N)}{\mathcal{N}}=\frac{2e^x}{1+2e^x} \quad (6)$$

for the average electron density $\bar{n}(T,\mu,N)=\partial\Omega(T,\mu,N)/\partial\mu$,

$$\frac{S(T,\mu,N)}{\mathcal{N}}=\ln(1+2e^x)-\frac{2xe^x}{1+2e^x} \quad (7)$$

for the entropy $S(T,\mu,N)=-\partial\Omega(T,\mu,N)/\partial T$, or the specific heat in the grand-canonical ensemble

$$\frac{C(T,\mu,N)}{\mathcal{N}}=\frac{T\,\partial S(T,\mu,N)}{\mathcal{N}\,\partial T}=\frac{2x^2e^x}{1+2e^x}-\left(\frac{2xe^x}{1+2e^x}\right)^2. \quad (8)$$

The specific heat at constant n vanishes identically, $C(T,n,N)=0$, as can be verified explicitly using the results (6)–(8) for $\bar{n}(T,\mu,N)$, $S(T,\mu,N)$, and $C(T,\mu,N)$. Equations (5)–(8) given above represent the contribution of the localized-electron states to the respective thermodynamic quantities. In Sec. V we will demonstrate that these analytic expressions are an excellent description of the thermodynamics of the full model at low temperatures.

The average ground-state electron number $\bar{n}(0,\mu,N)$ exhibits a jump from $\mathcal{N}$ to zero as μ exceeds μ_0. Moreover, at $\mu=\mu_0$ we have $x=0$ resulting in a finite residual entropy $S(0,\mu_0,N)/\mathcal{N}=\ln 3\approx 1.0986$. We note that thermodynamic quantities for all considered models are identical up to a factor $\mathcal{N}/N$ and the concrete value of μ_0, i.e., the low-temperature behavior is universal for the whole family of lattices constructed by the rules formulated in Sec. II.

V. NUMERICAL RESULTS

Let us now present numerical results obtained by exact diagonalization for finite lattices. We set $t=1$ for convenience. These calculations have been performed, on the one hand, to estimate the range of validity of the derived expressions for the low-temperature thermodynamics and, on the other hand, to study the states with $n>\mathcal{N}$ in more detail. The numerical effort to diagonalize the Hubbard model (1) grows rapidly with N. It is therefore convenient to consider also the limit $U\to\infty$ where doubly occupied sites can be eliminated from the Hilbert space. Computations were performed using different programs including Schulenburg's spinpack[20] and a custom implementation of the Householder algorithm.[21]

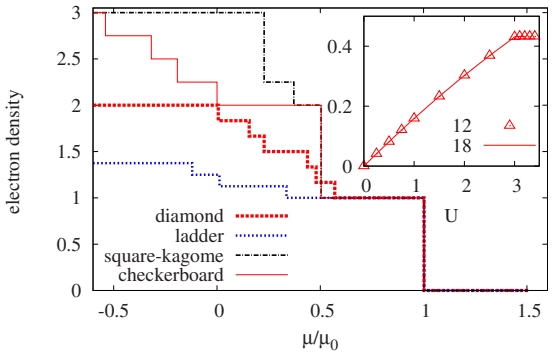

FIG. 2. (Color online) Electron density $\bar{n}/\mathcal{N}$ versus chemical potential μ/μ_0 for the diamond chain ($N=18$, $t'=3$), the frustrated ladder ($N=16$, $t'=3$), the square-kagome lattice ($N=24$, $t'=2$), and the checkerboard lattice ($N=16$, $t'=2$) for $U\to\infty$ and $T=0$. The universal dependence [Eq. (6)] at $T=0$ is given by $\theta(1-\mu/\mu_0)$. Inset: charge gap $\Delta\mu/\mu_0$ at $\bar{n}/\mathcal{N}=1$ versus U for the diamond chain [$N=12$ (triangles), $N=18$ (line), $t'=3$].

Note first that the degeneracies of the localized ground states calculated for various lattices and parameter sets perfectly fit to the prediction $g_{\mathcal{N}}(n)$ of Sec. III. The average electron density $\bar{n}/\mathcal{N}$ versus μ/μ_0 shown in Fig. 2 exhibits a jump between 0 and 1 at $\mu/\mu_0=1$ and a plateau at $\bar{n}/\mathcal{N}=1$ with the width $\Delta\mu/\mu$. The charge gap $\Delta\mu=E(\mathcal{N}+1)-2E(\mathcal{N})+E(\mathcal{N}-1)$ determines the region in which the localized states exclusively control the ground-state behavior of the model (1). The inset in Fig. 2 shows that $\Delta\mu$ is almost size independent. The charge gap increases almost linearly with U for small U, showing that this is a correlation effect. For the diamond chain with $t'=3t$, the charge gap saturates at $\Delta\mu\approx 0.43t$ for $U\gtrsim 3t$.

A. Thermodynamics for ideal geometry

Next we compare the specific heat $C(T,\mu,N)$ in the grand-canonical ensemble for the diamond chain, the frustrated ladder, the square-kagome lattice, and the checkerboard lattice at $\mu=0.95\mu_0$, μ_0, and $1.05\mu_0$ in the limit $U\to\infty$ (Fig. 3). $C(T,\mu,N)/\mathcal{N}$ versus T/μ_0 exhibits a universal additional low-temperature maximum for the chemical potential around μ_0. This low-temperature maximum emerges due to the manifold of localized-electron states, whose energies are slightly split for $\mu=0.95\mu_0$ and $1.05\mu_0$ but still well separated from energies of other higher energy states. Indeed, the low-temperature maximum is excellently described by the localized-electron formula (8) (lines in Fig. 3). Recall that the result (8) is valid for any N. Accordingly, there are no finite-size effects for the low-temperature maximum of the specific heat. In Fig. 3, one observes another maximum of $C(T,\mu,N)$ at higher temperatures. This maximum collects all states which are not localized-electron states and thus depends on details of the model. If $\mu\to\mu_0$ the low-temperature maximum shifts to lower T and is even much better separated from the high-temperature maximum. At $\mu=\mu_0$, we have $x=0$. Consequently, the contribution [Eq. (8)]

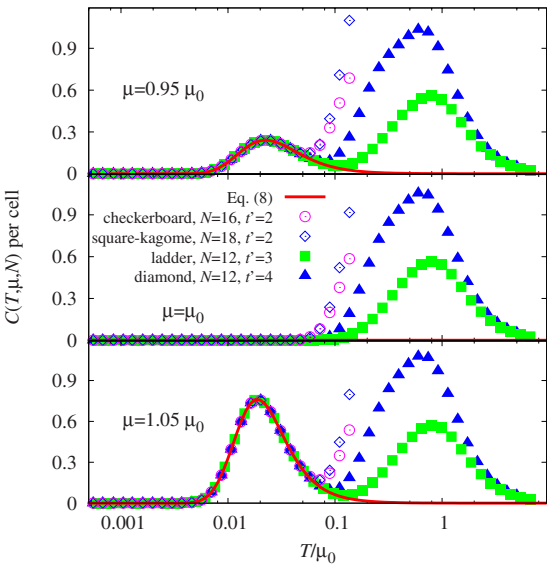

FIG. 3. (Color online) $C(T,\mu,N)/\mathcal{N}$ versus temperature T/μ_0 in the limit $U\to\infty$ for the diamond chain (triangles), the frustrated ladder (squares), the square-kagome lattice (diamonds), and the checkerboard lattice (circles). We also show the universal dependence [Eq. (8)] (lines).

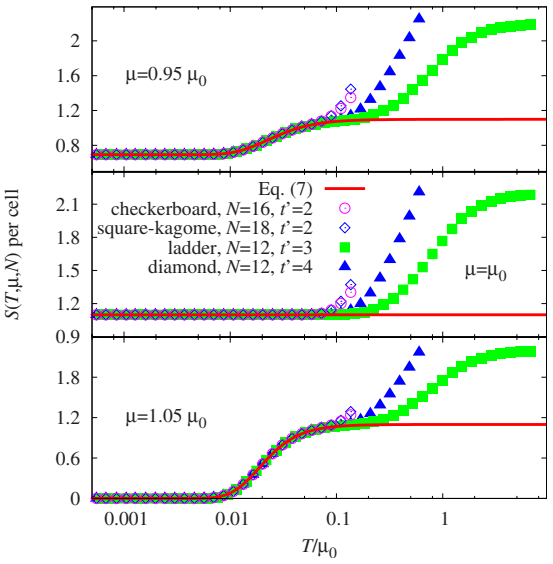

FIG. 5. (Color online) Entropy $S(T,\mu,N)/\mathcal{N}$ versus temperature T/μ_0 in the limit $U\to\infty$ for the diamond chain (triangles), the frustrated ladder (squares), the square-kagome lattice (diamonds), and the checkerboard lattice (circles). We also show the universal dependence [Eq. (7)] (lines).

of the localized-electron states to the specific heat C vanishes identically. Therefore, the temperature where the numerical data for $C(T,\mu_0,N)$ begin to deviate from zero (see the middle panel of Fig. 3) represents a characteristic temperature below which the localized states exclusively control the thermodynamic behavior of the model (1).

Figure 4 illustrates the influence of different values of U, using the example of the frustrated ladder with $N=12$ and $t'=3$. The low-temperature maximum in $C(T,\mu_0,N)$ is independent of U, as expected. By contrast, the high-temperature maximum does depend on U and it extends to lower temperatures for smaller values of U. Nevertheless, the localized-electron states are still well separated from the other states for the values of $U\geq 4$ and $\mu=0.95\mu_0$, $1.05\mu_0$ shown in Fig. 4.

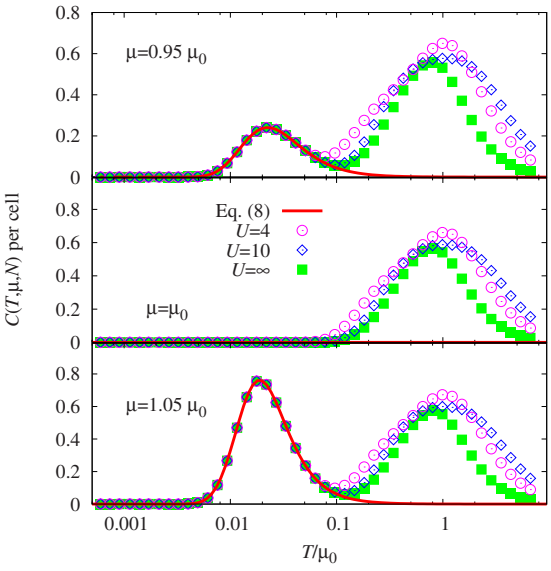

FIG. 4. (Color online) $C(T,\mu,N)/\mathcal{N}$ for the frustrated ladder with $N=12$ and $t'=3$ for different values of U. We also show the universal dependence [Eq. (8)] (lines).

Figure 5 shows the entropy S for the same lattices and parameters as in Fig. 3. Since $C(T,\mu,N)$ is a temperature derivative of $S(T,\mu,N)$, the features in the latter quantity correspond to those in the former. In particular a steep slope in $S(T,\mu,N)$ corresponds to a maximum of $C(T,\mu,N)$. However, there is one additional piece of information in $S(T,\mu,N)$, namely, its value in the low-temperature limit: for $\mu=\mu_0$, $S(T,\mu,N)/\mathcal{N}$ tends to $\ln 3\approx 1.0986$ for $T\to 0$ (see Sec. IV). If the chemical potential μ is in the charge-gap region, i.e., for $\mu_0-\Delta\mu<\mu<\mu_0$, the entropy per unit cell stays also finite for $T\to 0$ (compare the upper panel of Fig. 5). For these values of μ the ground state is the charge-ordered state (Wigner crystal) with $n=\mathcal{N}$ electrons and accordingly exhibits a ground-state degeneracy of $g_{\mathcal{N}}(\mathcal{N})=2^{\mathcal{N}}$ due to the independence of the spin orientations of the $\mathcal{N}$ electrons; see Eq. (4). Indeed, Eq. (7) shows that the entropy per cell $S/\mathcal{N}\to\ln 2\approx 0.6931$ when $x\to\infty$, i.e., $T\to 0$ and $\mu<\mu_0$.

B. Deviations from ideal geometry

In real compounds the conditions under which the localized states exist may be not strictly fulfilled. It is therefore important to study deviations from "ideal geometry". Such deviations or distortions in general lift the ground-state degeneracy. Nevertheless, one may expect that localized-state effects survive in a certain temperature range if the distortion is sufficiently small such that the originally degenerate energy levels remain close to each other. We investigate this issue in more detail using the example of the distorted dia-

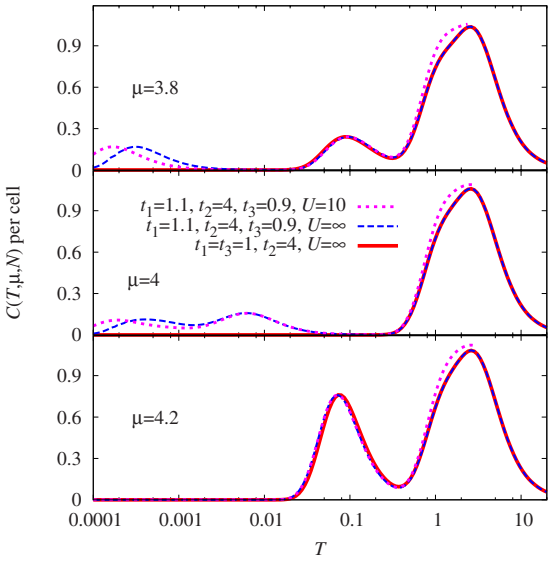

FIG. 6. (Color online) $C(T,\mu,N)/\mathcal{N}$ for the ideal diamond chain ($t'=4$, $t=1$) and the distorted diamond chain ($t_1=1.1$, $t_2=4$, $t_3=0.9$). The system size is $N=12$ in all cases.

mond chain ($N=12$, $t'=4$) where we distinguish the hopping terms running from north-west to south-east $t_1>t$ ($t_1=1.1$) and those running from south-west to north-east $t_3<t$ ($t_3=0.9$); see Fig. 1. This generalization is inspired by the set of exchange interactions proposed for azurite in Ref. 4. Figure 6 shows numerical results for $N=12$, $U=\infty$ and 10 in comparison to the data for the undistorted case which are identical to those shown in Fig. 3. The effect of the distortion is evidently very small for $T\gtrsim 0.04$. In particular, the additional low-temperature maximum in the grand-canonical specific heat $C(T,\mu,N)/\mathcal{N}$ for $\mu=3.8$ and 4.2 (corresponding to $\mu=0.95\mu_0$ and $1.05\mu_0$ in the undistorted case) is essentially unaffected. This implies that an important fingerprint of the highly degenerate localized states survives a small distortion. Additional features emerge in Fig. 6 for the distorted diamond chain in the region $T\lesssim 0.01$ at $\mu=3.8$ and for $T\lesssim 0.1$ at $\mu=4$. It is evident from Fig. 6 that these features depend on the value of U. Comparison with smaller system sizes for $U=10$ (not shown) exhibits also finite-size effects for $T\lesssim 0.001$ at $\mu=3.8$ and for $T\lesssim 0.01$ at $\mu=4$. One may therefore speculate that the additional low-temperature maximum observed in $C(T,\mu,N)$ for $\mu=4$ around $T\approx 0.006$ in Fig. 6 survives the thermodynamic limit, but it is difficult to infer the behavior in the thermodynamic limit at even lower temperatures.

The specific heat $C(T,n,N)$ in the *canonical* ensemble, i.e., for a fixed number of electrons n, may be particularly relevant from the experimental point of view. In Sec. IV we have already used the results for the grand-canonical ensemble to point out that the contribution of the localized-electron states to $C(T,n,N)$ always vanishes identically in the ideal situation. This is also evident if one considers a fixed number of electrons: in this case all localized n-electron states have the same energy E and using the representation $C=(\langle E^2\rangle-\langle E\rangle^2)/T^2$ in terms of the fluctuations of E one finds $C(T,n,N)=0$.

We use again the example of the (distorted) diamond chain to take a closer look at the behavior of $C(T,n,N)$. The

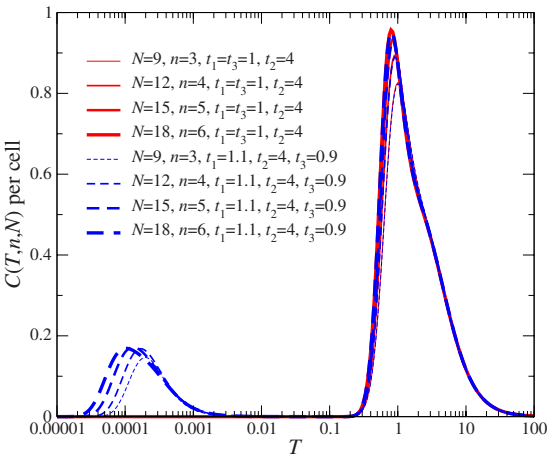

FIG. 7. (Color online) Specific heat $C(T,n,N)/\mathcal{N}$ for the ideal diamond chain ($t'=4$, $t=1$) and the distorted diamond chain ($t_1=1.1$, $t_2=4$, $t_3=0.9$) with $n=N/3$ electrons for $N=9,12,15,18$. The Hubbard repulsion is $U=10$.

case of the Wigner crystal, i.e., $n=\mathcal{N}$ may be particularly interesting. Figure 7 shows numerical results for the specific heat $C(T,n,N)/\mathcal{N}$ of both the ideal and the distorted diamond chains with $n=\mathcal{N}=N/3$ electrons. First, we observe that $C(T,n,N)$ of the ideal diamond chain (solid lines in Fig. 7) is indeed indistinguishable from zero for $T\lesssim 0.1$ and accordingly there is no low-temperature maximum. By contrast, for the distorted diamond chain the exact degeneracy of the ground-state manifold is removed, leading to the recovery of a low-temperature maximum. For the parameters used in Fig. 7, this low-temperature maximum appears at $T\approx 10^{-4}$ (see dashed lines in Fig. 7), reflecting the fact that the detuning $t_3=0.9\neq t_1=1.1$ leads only to a very small splitting of the originally 2^n-fold degenerate ground-state manifold. There is another high-temperature maximum at temperatures of order one in Fig. 7 where the results for the distorted diamond chain are indistinguishable from those for the ideal situation. The double-peak structure found in the canonical specific heat $C(T,n,N)$ of the distorted situation is qualitatively remarkably similar to the double-peak structure in the grand-canonical specific heat $C(T,\mu,N)$ observed, e.g., for $\mu=3.8$ in Fig. 6.

While finite-size effects are mostly unimportant in the grand-canonical ensemble, they are clearly relevant in the low-temperature region of Fig. 7 and visible even in the region of the high-temperature maximum. Such enhanced finite-size effects are typical for computations performed in the canonical ensemble where one considers only a fixed number of electrons n.

VI. MAGNETIC PROPERTIES

We return now to the ideal geometry and discuss ground-state magnetism. Since the trapping cells are independent of each other (i.e., they do not have common sites), the cells can be occupied independently by electrons with spin up or spin down for $n=1,\ldots,\mathcal{N}$. As a result, for $n\leq\mathcal{N}$ the majority of the degenerate ground states of the Hamiltonian (1) on

the considered lattices is nonmagnetic. Indeed, using the localized-electron picture of Sec. III, it is straightforward to show for the total spin operator $\boldsymbol{S}=(S^x,S^y,S^z)$ that

$$\frac{\langle \boldsymbol{S}^2\rangle_n}{N^2}=\frac{3\langle (S^z)^2\rangle_n}{N^2}=\frac{3n}{4N^2}\overset{N\to\infty}{\longrightarrow}0 \tag{9}$$

for $n\leq\mathcal{N}$, where the limit $N\to\infty$ is taken for a fixed electron density n/N. Here $\langle\cdots\rangle_n$ denotes the average over all ground states in the sector with n electrons.

The situation changes fundamentally at $n=\mathcal{N}+1$. If U is small (with respect to the energy gap between the flat band and the next band; this gap can be controlled by the ratio t'/t) an extra electron may lead to formation of a complicated many-body state with an energy that increases with growing U. However, if U is large enough, $U>U_c(\mathcal{N}+1)$, it might be energetically favorable to avoid double occupancy by putting one extra electron in the lowest-energy state of the next (dispersive) one-electron band in addition to the $\mathcal{N}$ localized electrons. The magnitude of U_c depends on the system under consideration. It is possible to find an explicit expression for such an eigenstate,

$$|\varphi_{\mathcal{N}+1}\rangle\propto\beta^\dagger_{\kappa_0,\uparrow}l^\dagger_{\mathcal{N},\uparrow}\ldots l^\dagger_{1,\uparrow}|0\rangle. \tag{10}$$

Here $\beta^\dagger_{\kappa_0,\sigma}$ creates an electron in the lowest dispersive band with momentum κ_0 and spin σ. The state $|\varphi_{\mathcal{N}+1}\rangle$ is fully polarized, i.e.,

$$\langle\varphi_{\mathcal{N}+1}|\boldsymbol{S}^2|\varphi_{\mathcal{N}+1}\rangle=\frac{\mathcal{N}+1}{2}\left(\frac{\mathcal{N}+1}{2}+1\right), \tag{11}$$

and it has a U-independent energy $\mathcal{N}\varepsilon_1+\varepsilon_2(\kappa_0)$. Other states belonging to a spin-$\frac{\mathcal{N}+1}{2}$ SU(2) multiplet can be obtained by applying $S^-=\Sigma_i c^\dagger_{i,\downarrow}c_{i,\uparrow}$ to this state (Kramers degeneracy). This multiplet can also be obtained by applying $S^+=\Sigma_i c^\dagger_{i,\uparrow}c_{i,\downarrow}$ to the spin-down counterpart of Eq. (10).

Numerically, we find such ferromagnetic ground states for large U also for bigger $\mathcal{N}<n<N$. For finite systems the numbers of electrons n for which ferromagnetic ground states appear depend on the lattice size and the boundary conditions.[22,23] For all lattices considered in this paper and the imposed periodic boundary conditions we find fully polarized ground states for particular values of the electron number $n>\mathcal{N}$ for sufficiently large $U>U_c$. In Table I we list some combinations of finite lattices and numbers of electrons n for which the ground state is fully polarized for $U\to\infty$. Note that the state (10) is incompatible with the boundary conditions of the $N=24$ square-kagome and the $N=16$ checkerboard lattices such that there is no saturated ground-state ferromagnetism for $n=5$ on these two lattices. In addition, we give as an example the strength of correlation $U>U_c$ that is needed to realize ground-state ferromagnetism for $n=\mathcal{N}+1$ for the frustrated ladder with $N=16$ sites; we found $U_c\approx 0.42$ and 12.78 for $t'=2.1$ and 4, respectively.

This kind of ferromagnetism that occurs only for sufficiently strong on-site repulsion (note that it is not flat-band ferromagnetism that occurs for any $U>0$) was discussed also earlier for some one-dimensional systems.[16,22,23] Moreover we mention that the saturated ferromagnetism found for the largest electron number $n=N-1$ corresponds to Nagaoka's well-known result.[10,24] However, we emphasize that the occurrence of ferromagnetism for other electron numbers in the range $\mathcal{N}<n<N$ is a generic feature of the considered lattices and is therefore not restricted to one-dimensional systems.

TABLE I. Number of electrons $n>1$ for which there is a unique saturated ferromagnetic ground-state multiplet in the limit $U\to\infty$ on the specified lattice subject to periodic boundary conditions. Note that saturated ground-state ferromagnetism for the considered lattices of N sites occurs only for a sufficiently large number of electrons $\mathcal{N}<n<N$ (apart from the trivial case $n=1$). Note that for the square-kagome lattice with $N=24$ sites the ground states for $n=16,17,18,19$ have not been calculated because of the large size of the Hamiltonian matrix.

Lattice	Number of electrons
Diamond, $N=12$ ($\mathcal{N}=4$)	$n=5,7,8,9,11$
Diamond, $N=18$ ($\mathcal{N}=6$)	$n=7,9,11,12,13,15,17$
Ladder, $N=12$ ($\mathcal{N}=6$)	$n=7,9,11$
Ladder, $N=16$ ($\mathcal{N}=8$)	$n=9,11,13,15$
Square-kagome, $N=18$ ($\mathcal{N}=3$)	$n=4,5,7,8,15,17$
Square-kagome, $N=24$ ($\mathcal{N}=4$)	$n=7,8,9,\ldots,20,21,23$
Checkerboard, $N=16$ ($\mathcal{N}=4$)	$n=7,8,9,15$

VII. CONCLUSIONS

In summary, we have given an exact solution for the ground-state properties of a correlated many-electron system on a class of lattices in a certain range of the chemical potential μ. We have studied the low-temperature thermodynamics which for μ around μ_0 is controlled just by the manifold of localized ground states. In particular, we have presented explicit expressions for the low-temperature behavior of the grand-canonical partition function and related quantities such as the grand-canonical specific heat $C(T,\mu,N)$. The localized-electron features have no finite-size effects and are universal, i.e., they are the same for the whole class of lattices.

Apart from the high-temperature maximum that is typical for systems with a bounded energy spectrum we find an additional low-temperature maximum in $C(T,\mu,N)$ if the chemical potential μ deviates slightly from μ_0. This extra maximum survives under small deviations from ideal lattice geometry. Moreover, for the canonical specific heat $C(T,n,N)$ the lifting of degeneracy caused by deviations from ideal lattice geometry actually *gives rise* to an additional low-temperature maximum in the specific heat. Thus, any splitting of the highly degenerate localized electron states, be it by a deviation of the chemical potential from μ_0 or by a deviation from ideal lattice geometry, leads to an extra low-temperature maximum in the specific heat as a characteristic fingerprint of the localized-electron states.

Furthermore, we argued that in contrast to the flat-band ferromagnets[10] there is no ground-state ferromagnetism in the present class of models if the electron density satisfies

$n/\mathcal{N} \leq 1$. For electron numbers $\mathcal{N} < n < N$ we observe saturated ground-state ferromagnetism for all considered lattices, including square-kagome and checkerboard lattices. An explicit expression for the saturated ferromagnetic ground state in the sector $n=\mathcal{N}+1$ is given in Eq. (10).

Finally we note that the t-J model on the considered lattices may exhibit similar localized ground states in the subspaces with $n=1,\ldots,\mathcal{N}$ electrons for values of the spin-exchange interaction J up to about the hopping integral t. Another interesting variation in the considered models refers to multiorbital systems.[9] For instance, the one-orbital Hubbard model on a frustrated ladder can be related to a two-orbital Hubbard model on a simple chain with a hybridization term corresponding to the hopping on a rung. This relation between one-orbital models and multiorbital models extends the region of applicability of the localized-states scenario.

ACKNOWLEDGMENTS

We thank J. Jędrzejewski for discussions. O.D. acknowledges the financial support of the DAAD. Financial support of the DFG is gratefully acknowledged (Project No. RI 615/18-1 and a Heisenberg Grant for A.H. under Project No. HO 2325/4-1).

[1] C. K. Majumdar and D. K. Ghosh, J. Math. Phys. **10**, 1388 (1969).
[2] B. S. Shastry and B. Sutherland, Physica B & C **108**, 1069 (1981).
[3] A. Kitaev, Ann. Phys. **321**, 2 (2006).
[4] H. Kikuchi, Y. Fujii, M. Chiba, S. Mitsudo, T. Idehara, T. Tonegawa, K. Okamoto, T. Sakai, T. Kuwai, and H. Ohta, Phys. Rev. Lett. **94**, 227201 (2005).
[5] R. Arita, Y. Suwa, K. Kuroki, and H. Aoki, Phys. Rev. Lett. **88**, 127202 (2002); Y. Suwa, R. Arita, K. Kuroki, and H. Aoki, Phys. Rev. B **68**, 174419 (2003).
[6] A. Harrison, J. Phys.: Condens. Matter **16**, S553 (2004).
[7] M. Ichimura, K. Kusakabe, S. Watanabe, and T. Onogi, Phys. Rev. B **58**, 9595 (1998); H. Tamura, K. Shiraishi, T. Kimura, and H. Takayanagi, *ibid.* **65**, 085324 (2002); H. Ishii, T. Nakayama, and J.-i. Inoue, *ibid.* **69**, 085325 (2004).
[8] M. Lewenstein, A. Sanpera, V. Ahufinger, B. Damski, A. Sen, and U. Sen, Adv. Phys. **56**, 243 (2007).
[9] C. Wu, D. Bergman, L. Balents, and S. Das Sarma, Phys. Rev. Lett. **99**, 070401 (2007); C. Wu and S. Das Sarma, Phys. Rev. B **77**, 235107 (2008).
[10] H. Tasaki, Prog. Theor. Phys. **99**, 489 (1998) and references therein.
[11] C. D. Batista and B. S. Shastry, Phys. Rev. Lett. **91**, 116401 (2003).
[12] J. Schulenburg, A. Honecker, J. Schnack, J. Richter, and H.-J. Schmidt, Phys. Rev. Lett. **88**, 167207 (2002); J. Richter, J. Schulenburg, A. Honecker, J. Schnack, and H.-J. Schmidt, J. Phys.: Condens. Matter **16**, S779 (2004).
[13] More general trapping cells such as nonbipartite cells or cells with nonequivalent sites and bonds are possible as well, cf. Refs. 11 and 19.
[14] J. Vidal, B. Douçot, R. Mosseri, and P. Butaud, Phys. Rev. Lett. **85**, 3906 (2000); Z. Gulácsi, A. Kampf, and D. Vollhardt, *ibid.* **99**, 026404 (2007); arXiv:0806.0289(unpublished).
[15] I. Bose and S. Gayen, Phys. Rev. B **48**, 10653 (1993).
[16] A. Tanaka and T. Idogaki, J. Phys. Soc. Jpn. **67**, 401 (1998).
[17] M. E. Zhitomirsky and H. Tsunetsugu, Phys. Rev. B **70**, 100403(R) (2004); O. Derzhko and J. Richter, *ibid.* **70**, 104415 (2004); M. E. Zhitomirsky and H. Tsunetsugu, Prog. Theor. Phys. Suppl. **160**, 361 (2005); O. Derzhko and J. Richter, Eur. Phys. J. B **52**, 23 (2006).
[18] H.-J. Schmidt, J. Richter, and R. Moessner, J. Phys. A **39**, 10673 (2006).
[19] O. Derzhko, A. Honecker, and J. Richter, Phys. Rev. B **76**, 220402(R) (2007).
[20] http://www-e.uni-magdeburg.de/jschulen/spin/
[21] A. Honecker and J. Schüle, in *Advances in Parallel Computing*, edited by C. Bischof, M. Bücker, P. Gibbon, G. R. Joubert, T. Lippert, B. Mohr, and F. Peters (IOS Press, Amsterdam, 2008), Vol. 15, pp. 271–278.
[22] Y. Watanabe and S. Miyashita, J. Phys. Soc. Jpn. **66**, 2123 (1997); **66**, 3981 (1997); **68**, 3086 (1999).
[23] R. Arita and H. Aoki, Phys. Rev. B **61**, 12261 (2000).
[24] Y. Nagaoka, Phys. Rev. **147**, 392 (1966).